

1 **Running Title:** *Drosophila* descending neuron function

2

3 **Title**

4 Optogenetic dissection of descending behavioral control in *Drosophila*.

5

6 **Authors**

7 Jessica Cande^{1*}, Gordon J. Berman^{2,3*}, Shigehiro Namiki^{1,4}, Jirui Qiu³, Wyatt Korff¹,
8 Gwyneth Card¹, Joshua W. Shaevitz⁵ and David L. Stern¹.

9

10 **Author Affiliations**

11 ¹Janelia Research Campus, Howard Hughes Medical Institute, Ashburn, VA 20147.

12 ²Department of Biology, Emory University, Atlanta, Georgia 30322.

13 ³Department of Physics, Emory University, Atlanta, Georgia 30322.

14 ⁴Research Center for Advanced Science and Technology, University of Tokyo, Tokyo
15 153-8904, Japan.

16 ⁵Department of Physics and the Lewis-Sigler Institute for Integrative Genomics,
17 Princeton University, Princeton, New Jersey 08544.

18 *These authors contributed equally to the manuscript.

19

20 **Correspondence (for submission purposes):** David L. Stern

21 Email: sternd@janelia.hhmi.org

22 Telephone: 571-209-4237

23 19700 Helix Dr., Ashburn, VA 20147

Abstract

In most animals, the brain makes behavioral decisions that are transmitted by descending neurons to the nerve cord circuitry that produces behaviors. In insects, only a few descending neurons have been associated with specific behaviors. To explore how these neurons control an insect's movements, we developed a novel method to systematically assay the behavioral effects of activating individual neurons on freely behaving terrestrial *D. melanogaster*. We calculated a two-dimensional representation of the entire behavior space explored by these flies and associated descending neurons with specific behaviors by identifying regions of this space that were visited with increased frequency during optogenetic activation. Applying this approach across a population of descending neurons, we found, that (1) activation of most of the descending neurons drove stereotyped behaviors, (2) in many cases multiple descending neurons activated similar behaviors, and (3) optogenetically-activated behaviors were often dependent on the behavioral state prior to activation.

Introduction

As animals navigate a dynamic environment, their survival depends on their ability to execute specific motor programs and to adjust motor output in response to external stimuli. While the brain performs computations essential for behavior, the motor circuits that directly control behavior are located close to the muscles that they control in the vertebrate spinal cord and insect ventral nerve cord. Information to drive motor patterns must therefore be transmitted from the brain to the nerve cord to direct behavior. Since there are many fewer descending neurons than neurons in the central brain, descending neurons generate an information processing bottleneck, which may generate a fundamental problem in information coding.

In flies, descending commands from the brain to the ventral nerve cord are transmitted through an estimated 250-550 pairs of descending neurons that arborize in 20 highly-conserved clusters in the brain involved in sensory processing and motor behavior (Gronenberg & Strausfeld, 1990; Hsu & Bhandawat, 2016). Each descending neuron extends a single axon through the neck connective to the ventral nerve cord, where they synapse onto interneurons associated with leg, neck, and wing motor circuitry (Namiki et al, 2017).

Little is known about how so few neurons—approximately 0.5% of all neurons in the fly (Alivisatos et al., 2012)—encode signals from the brain to control the full range of movements performed by a freely moving fly. Several potential models have been suggested. One possibility is that, as with vertebrates, many stereotypical insect behaviors, such as walking, flying, or “singing” can be decomposed into individual motor modules controlled by central pattern generators located in the ventral nerve cord.

Several recent findings in *Drosophila melanogaster*, together with earlier electrophysiological studies in larger insects, support this idea. Activation of some individually-identifiable descending neurons triggers specific motor outputs, such as courtship song (von Philipsborn et al., 2011a), backwards walking (Bidaye, Machacek, Wu, & Dickson, 2014), or escape behavior (King & Wyman, 1980). However, some descending neurons modify motor programs, rather than trigger them. For example, cricket walking initiation, speed, and turning appear to depend on separately encoded descending commands (Böhm & Schildberger, 1992; Gras & Kohstall, 1998). Alternatively, motor activity may result from the summed activity of multiple descending neurons (Heinrich, 2002). For example, a cluster of descending neurons linking fly visual centers in the brain to the flight apparatus in the ventral nerve cord (Strausfeld & Gronenberg, 1990; Namiki et al, 2017) supports the idea that at least some descending neurons may function this way.

Descending neuron function may also be gated by behavioral state. For example, a single descending neuron may cause a different or modified behavior if the animal is walking versus flying. For example, DN sensory responses have been shown to be modified by locomotor state (Staudacher & Schildberger, 1998). This kind of gating has been observed in other contexts, such as the effect of the neuromodulator pyrokinin on the oscillatory mechanisms underlying the crustacean gastric mill central pattern generator (Marder & Goaillard, 2006). However, it has not previously been possible to undertake a systematic analysis of the context dependency across the DN population.

Systematic dissection of descending motor control is challenging for two reasons. First, it has been difficult to precisely manipulate a large number of descending neurons

individually in freely behaving animals. Second, we have not had a high-throughput, unbiased behavioral phenotyping pipeline capable of objectively categorizing all of an individual's movements. Historically, insect descending neuron anatomy, connectivity and function have been described by backfilling neurons with dye and recording from individual neurons in locusts, grasshoppers, and cockroaches (for a review see (Strausfeld, Bassemir, & Singh, 1984)), with more recent studies performing similar experiments in flies (Hsu & Bhandaway, 2016). While this approach has allowed researchers to describe the anatomy and electrophysiological responses of individual neurons, it is inherently low throughput and biased towards larger or otherwise more accessible neurons. Additionally, because experiments are typically carried out on immobile preparations, only in rare cases have investigators been able to link individual neurons to behavior (e.g. (E. Staudacher & Schildberger, 1998)). While recent technical and genetic advances in the model fly *Drosophila melanogaster* have improved our ability to access and manipulate individual descending neurons, to date only a handful of *Drosophila* descending neurons have been linked to specific motor outputs (e.g. (Bidaye et al., 2014; von Philipsborn et al., 2011b; von Reyn et al., 2014)).

To assess how descending neurons control motor behaviors on a systems scale, it will be necessary to move beyond isolated examples and to describe the behavioral functions of large numbers of descending neurons. Our goal was to identify all of the behavioral phenotypes observable in one particular setting, freely behaving flies moving within a two-dimensional arena, for many descending neurons, without any *a priori* expectation about the neurons' effects on behavior. Namiki et al (Namiki et al, 2017) created a collection of transgenic *Drosophila* strains that target descending neurons using

the split-GAL4 intersectional system (Pfeiffer et al., 2010) in a cell-type specific manner. We screened 130 of the sparsest lines in this collection, targeting approximately 160 neurons that are divisible into 58 distinct anatomical cell-types. 40 of these cell types consist of a single pair of bilaterally symmetric descending neurons, while the remaining 18 categories target populations of 3 to 15 descending neurons with similar neuroanatomy. We used this split-GAL4 collection to drive the expression of the red-shifted channelrhodopsin *CsChrimson* (Klapoetke et al., 2014a) in specified subsets of descending neurons, allowing us to photo-activate these neurons in a temporally precise fashion. We combined these genetic reagents with a recently described method for objective, quantitative analysis of behavior (Berman, Choi, Bialek, & Shaevitz, 2014) to comprehensively identify the behaviors associated with the activation of specific neurons in an unbiased fashion. Unlike supervised machine learning approaches for classifying behavior, this approach does not rely on a human-trained classifier to decide which behaviors are of interest. Instead it captures a wide range of movements by converting high-dimensional postural dynamics into a two-dimensional map using dimensionality reduction techniques (Berman et al., 2014). Using this method, we associated 80% of the descending neurons in our collection with specific behaviors.

We have generated a behavioral dataset from freely walking animals that comprehensively describes the activation phenotypes of roughly one third to one half of the total number of fly descending neurons. The size of this dataset has allowed us to move beyond individual examples to extract general features of descending neuron function, and therefore to consider how these neurons might encode information to modulate behaviors. We find that, with a few exceptions, descending neuron control of

behavior appears to be largely modular. In addition, we find many cases in which descending neuron function is context dependent, even within the confines of a single fly confined to a two-dimensional substrate.

Results

Establishing a framework for large scale analysis of descending neuron activation phenotypes

Mapping fly behavior using postural dynamics requires high temporal and spatial resolution video data from a large number of animals. Accordingly, we built a red light activation apparatus that consisted of an array of 12 USB cameras that allowed us to film 12 flies in separate chambers simultaneously at high resolution (Figure 1A). We crossed each split-GAL4 line to a UAS-CsChrimson line, and we filmed six experimental progeny that had been fed retinal, a co-factor necessary for neuronal activation via channelrhodopsin, and six genetically identical control flies whose food had not been supplemented with retinal. The flies were backlit using custom light tables, each consisting of an array of infrared and red LEDs covered by a diffuser. Each chamber was a 3 cm “fly bubble” (Klibaite (2017)), which had sloping sides coated with silicone. This encouraged the flies to remain on the flat floor of the chamber, where they could roam freely and would remain in the focal plane of the camera (Berman et al., 2014). For each split-GAL4 line, we recorded 30 trials consisting of a 15-second pulse of red light followed by a 45 second recovery interval (Figure 1A).

If the descending neuron(s) labeled by a particular split-GAL4 line are involved in triggering, maintaining, or modulating a particular behavior, then activating these

neurons with *CsChrimson* may be sufficient to activate that behavior. To identify behavioral phenotypes in an unbiased manner, we utilized the behavior mapping methods described in Berman et al. (2014). First, we generated a comprehensive “behavior space” of stereotyped actions that single flies could produce in our assay. We collected a dataset of approximately 700 million images, which included behaviors recorded from activation of descending interneuron split-GAL4 lines, previously characterized sparse GAL4 drivers (*fruitless-GAL4* and *pIP10*) that trigger courtship-related behaviors (Stockinger, Kvitsiani, Rotkopf, Tirián, & Dickson, 2005; von Philipsborn et al., 2011b), and interneuron drivers targeting the flight neuropil. The additional lines that are not part of the descending neuron screen were included to sample fly behaviors as widely as possible, allowing for higher resolution mapping within the space of behaviors. We computed the behavior space by (1) aligning video images (Figure 1A), (2) decomposing the pixel value dynamics (which correspond to the fly’s posture changes) into a low-dimensional basis set using principal component analysis (Figure S1), (3) projecting the original pixel values onto this basis set and transforming those values using a spectral wavelet function to produce a time series that was (4) embedded into a two-dimensional “behavior space” (Figure 1B) using *t*-distributed Stochastic Neighbor Embedding (t-SNE) (van der Maaten & Hinton, 2008).

Each position in the behavior space corresponds to a unique set of postural dynamics. Nearby points represent similar motions, i.e. those involving related body parts executing similar temporal patterns. By observing the video data underlying subregions of the behavior space (Figure S2 and movies S1-S5), we generated a human-curated version of the behavior space to aid interpretation (Figure 1C). In this behavior

space, anterior directed movements such as eye/antennal grooming and proboscis extension are located at the top (supplemental movie S1). Anterior-directed foreleg movements are on the upper left side (movie S2). Extremely slow or still postures are on the upper right side (movie S3), and complex wing and abdomen movements such as body and abdomen grooming, abdomen bending and wing extension are in the center (movie S4). Locomotion, ranging from slow (left) to fast (right) is at the bottom (movie S5).

Red peaks, or density maxima, represent the fly behaviors observed most frequently in our data set. These tend to be repetitive, stereotyped behaviors, such as walking or grooming, that our analysis methodology is most sensitive at detecting. By definition, we could not detect behaviors occurring over time-scales faster than 50 Hz, the Nyquist frequency of our system. Approximately 93% of all video image data points could be embedded in this space, irrespective of whether the red light was on or off (Figure S3), indicating that the majority of red light activated behaviors are well represented in the behavior space. Un-embeddable imaging errors, such as the fly wandering partially out of frame, are randomly distributed within the dataset.

Entropy of behavior space density provides a quantitative and sensitive measure of optogenetic activation phenotypes

Having established a behavior space representing the full repertoire of fly behaviors that could be captured with our apparatus, we next examined which parts of this space were occupied when individual or subsets of descending neurons were optogenetically activated by CsChrimson. We focused on 130 split-GAL4 lines that

targeted descending neurons with little, or no, extraneous expression in other neurons. We first considered the timing and duration of red light triggered behaviors. If descending neuron activation triggered a particular behavior represented in the behavior space, then we expect that the density of that line in the behavior space should shift into the region that represents that behavior during periods of red light activation. For example, upon red light activation, retinal-fed flies expressing *CsChrimson* in a descending neuron line targeting DNg07 and DNg08 (SS02635) groomed their heads (supplemental movie S6). We identified regions in the behavior space that experienced a statistically significant shift in density for experimental flies during the first three seconds of red light compared to a window at the end of the recovery period when the red light was off (Figure 2B, C, Figure S4). This same region in the behavior space did not undergo a significant shift in the control flies (Wilcoxon rank-sum test $p < 0.05$ using the Dunn–Šidák correction for multiple hypotheses (Šidák, 1967)). Likewise, when considering densities over the whole behavior space in three second sliding windows, the experimental, but not the control, flies shift into the head grooming region (arrowheads, Figure 2C).

The shift in behavior in the experimental animals, and the timing of this shift relative to red light activation, can be detected as a reduction in the entropy of the behavior space density during this epoch (Figure 2A). Entropy measures the degree of disorder inherent in the distribution of the flies in the behavior space. When the red light was off, flies exhibited a range of different behaviors, and the probability that they performed any one behavior was low. This results in a low probability density distributed throughout the behavior space and correspondingly high entropy (Figure 2A).

Upon red light activation, the experimental fly line engaged in red light triggered behaviors at the expense of other natural behaviors. This increased the probability that they occupied a small region within the behavior space, generating a drop in entropy whose timing and duration mirrored that of the red light triggered behaviors (Figure 2A movie S7). We can therefore use entropy as a proxy for the duration and onset of red light triggered movements in the behavior space without needing to know, *a priori*, which behaviors are activated (i.e. which part of the behavior space to examine).

The region density and entropy are quantitative measurements sensitive to small changes in behavior map distribution. We therefore used these values to identify subtle phenotypes that could not be easily identified by manual inspection of the movies. For example, the rapid activation of descending neuron DN_g25 induced a transient rapid running phenotype (Figure 2E & 2F) that was identified by the transient drop in entropy in the behavior space (Figure 2D) and the transient increase in density in the fast locomotion region of the space (Figure 2E & 2F, supplemental movie S8).

Comprehensive characterization of descending neuron split-Gal4 line activation phenotypes

To characterize the time-course and likelihood of optogenetically-induced phenotypes across the entire collection of descending neuron lines, we examined the entropy time course of each line (Figure 3). We found that most lines displayed the largest entropy drop immediately after red light activation (Figure 3A). For roughly a third of the lines, this entropy drop persisted throughout the entire red light activation window (Figure 3B). For most of the rest of the lines, however, the entropy drop was

transient and diminished after several seconds (Figure 3B). For a minority of lines, the entropy minimum occurred near the middle or end of the activation window (Figure 3B). We reviewed the raw video data for these lines and found that most of these flies performed some action upon red light activation, followed by a freeze. This explained why the entropy was lower in the later part of the activation window, because consistent stillness is a low entropy state (see Figure S5 for a line by line description of phenotypes). We therefore performed our system-wide analysis using the first 3 seconds of the red light activation period, because this time period captured the majority of CsChrimson activated behaviors.

In our initial analysis, we looked for behaviors produced when our descending neuron lines were activated using a comparatively low level of red light, (5 mW/cm²). Under these conditions, 91 of the 130 lines (69%) displayed a statistically significant increase in density of some area of the behavior space. We then re-tested most of the 41 lines that did not produce a significant density increase by driving CsChrimson at higher levels by growing the flies on food containing an increased retinal concentration and exposing flies to higher intensity red light (9 mW/cm²). Under these conditions, 80% of the lines that had previously displayed no phenotype produced a statistically significant increase in density in the behavior space.

Pooling the data from the low and high activation protocols, we detected statistically significant increases in the behavior space in 119 of the 130 (90%) descending neuron lines (Figure 4A). In 86 cases, we observed an increased density in only a single statistically significant region in the behavior space. However some lines generated density increases in multiple non-contiguous regions of the behavior space

(Figure 4A, examples shown in Figure 4B-D, supplemental movies S9-S11, supplemental figure S5). In many cases, these multi-region lines reflect multiple behaviors performed approximately simultaneously by the flies. For example, a line targeting DNp10 induced anterior reaching movements and wing flicking with similar timing (Figure 4D, red and blue regions respectively). However, in other cases, multiple activated regions reflect a stereotyped sequence of behaviors. For example, the DNp09 line shown in Figure 4B repeatedly ran and then paused throughout the entire 15 second activation period. The increased density in the run region of the behavior space (Figure 4B, red) appeared before the increased density in the paused region (Figure 4B, blue), reflecting the sequential timing of the two behaviors. However, the flies rapidly became asynchronous as they repeated this series of behaviors, so this behavioral series is detected as density increases in the running and still regions throughout the red light activation window. A line targeting descending neuron DNb01 displayed a simple behavior series; flies produced an anteriorly directed twitch of the front legs when the red light was turned on (Figure 4C, red region), then froze for the majority of the red light activation period (Figure 4C, black region), and then twitched when the light was turned off (Figure 4C, blue region). Thus, examining the timing of density shifts illuminates the more complicated behavior series produced by red light activation. This level of analysis is provided for all lines in supplemental Figure S5.

Behavioral result of descending neuron activation is often context dependent

Why does activation of some descending neurons result in multiple, distinct behavioral outputs? One possibility is that the behavioral output of some descending

neurons depends on the behavioral context of the fly when the descending neuron is activated. To address this possibility, we calculated the mutual information between the density distribution of the experimental flies in the behavior space at 1.5 to 0.5 seconds before the red light was turned on versus the first second after red light activation. Mutual information is a non-linear measure of the degree of dependence between two variables and is typically measured in units of bits (Cover & Thomas, 2005). The higher the mutual information, the more the first variable, here the behavior of flies immediately prior to red light activation as measured by their distribution in the behavior space at $t = -1.5$ to -0.5 seconds, informs the value of the second variable, the region of the behavior space occupied in the first second of red light activation.

We found that, in all cases, experimental animals displayed non-zero mutual information between the pre- and post-stimulation behaviors (Figure 5A). In addition, for most lines, more information was available in the experimental flies than in the controls (Figure 5B). This means that even in those cases where red light activation produced only one significant region in the behavior space, the fly's activity prior to red light activation influenced whether or not it performed the behavior. However, lines with multiple red light activated regions in the behavior space were also those with a relatively high level of mutual information (Figure 5A-B). Thus, a given fly's behavior before red light activation was highly informative of which behavior that fly would perform after red light activation, as indicated by the different significantly activated regions in the behavior space. Figure 5C displays this phenomenon for one of the lines with the highest mutual information, SS02542 (asterisk in figure 5A-B, also shown in Figure 4C). Here, if the flies were performing an action in the wind/abdomen movement regions of the

behavior space prior to the stimulation, they were likely to perform an anterior movement (region 1) immediately following stimulation. Similarly, flies performing anterior grooming were likely to transition to the small anterior twitch region (region 2), and flies that were initially still tended to remain still post-stimulation (region 3).

Individual descending neurons produce mainly stereotyped, modular behaviors

So far, we have analyzed split-GAL4 lines as if they were a proxy for individual descending neurons or anatomical classes of descending neurons. However, these lines vary in both their strength of expression and in the number and identity of additional cells labeled. To estimate phenotypes for individual descending neurons, we therefore averaged the behavior space densities of multiple lines for those cases where we had multiple lines targeting the same descending neuron (Figure 6). Using this method, and combining it with those descending neurons for which we had only a single representative split-GAL4 line, we estimated phenotypes for 47 of the 58 descending neuron cell types. We have also included six lines and line averages that target two different types of descending neurons cleanly, but for which we have no lines that target each type individually. Twenty-six descending neurons drove locomotion phenotypes and ten drove anterior directed foreleg movements. We also identified six new descending neurons that triggered wing and abdomen movements (plus the previously published pIP10 (von Philipsborn et al., 2011b)), two that drove anterior grooming, one that drove abdomen stroking, and four that drove still or slow behaviors.

In general, we found that activation of each type of descending neuron drove behaviors that mapped to a relatively small region of the behavior space. For example, some descending neurons drove slow locomotion, whereas others drove fast locomotion.

Only a few, such as DNa01, DNa02 and DNp26, seemed to produce a global increase in locomotor activity. Likewise, we found descending neurons that produced different types of grooming, such as head grooming (DNg07 & DNg08, and DNg12) or abdomen grooming (DNp29), different types of anterior reaching movements (DNg10 versus DNg13) and different types of slow movements (e.g. DNd02 versus DNp02).

Discussion

Using optogenetic activation and automated behavioral quantification, we assigned behavioral phenotypes to 80% of the descending neurons cell types in our collection of lines, or one third to one half of the estimated total number of descending neurons present in the fly. Using a dataset of this scope, it is possible for the first time to move beyond isolated examples to consider systems-level trends in how descending neurons control behaviors.

For several reasons, this is unlikely to be a comprehensive categorization of the activation effects of these descending neurons. First, behaviors performed more quickly than the Nyquist frequency of 50Hz for our movies could not be detected. Second, we assayed only behaviors that can be activated when flies are standing and walking. Descending neurons controlling behaviors gated by flight, for example, would not be detected. Third, we assayed only males, so any female-specific behaviors may not be identified. Finally, we assayed solitary flies, so any behaviors gated by social interactions, for example courtship, may not have been detected.

There are several, non-mutually exclusive ways a limited number of seemingly highly modular descending neurons could encode the wide range of behaviors undertaken

by freely moving animals. First, descending neurons could be more important for triggering and maintaining behaviors than for controlling individual details of a given motor program (Heinrich, 2002). Many motor programs, particularly those controlling repetitive, rhythmic actions such as walking or stridulation, can function in the absence of descending control ((Bentley, 1977; Kien, 1983), for a review on walking circuits see (Ritzmann & Bü Schges, 2007)). For example, Hedwig (1994) identified two pairs of descending neurons that control stridulation in grasshoppers. In this system, tonic activation of the descending neurons was sufficient to induce and modulate the activity of the stridulation central pattern generator in the thorax, indicating that the descending neurons play only a limited role in patterning stridulation. Several of our lines, including the DNg07 & DNg08 head grooming line (Figure 2A & 2B), appear to reflect a similar phenomenon, driving a repeated stereotyped behavior during the entire CsChrimson activation window.

Second, behaviors might be controlled not by single descending neurons acting as command neurons, but by combinations of descending neurons acting in concert (Heinrich, 2002). Neuroanatomy suggests this possibility; roughly a third of described descending neurons appear to have unique projection patterns in *Drosophila* and *Calliphora*, while the rest share common input and/or output regions in the brain and ventral nerve cord with other descending neurons (Gronenberg & Strausfeld, 1990; Milde & Strausfeld, 1990; Namiki et al, 2017). In addition, several examples illustrate that multiple descending neurons control the same specific behaviors (Griss & Rowell, 1986; Gronenberg & Strausfeld, 1990; Hensler, 1992; Kanzaki, Ikeda, & Shibuya, 1994; Kien, 1983, 1990; Milde & Strausfeld, 1990; Rowell & Reichert, 1986; E. M. Staudacher,

2001). In this case, Larimer et al (1988) suggest that sufficiently strong stimulation of one neuron in a command cohort or module is sufficient to recruit the activity of the other descending neurons, triggering the behavior. Our data do not allow us to definitively address this question. However, the large number of descending neurons that drive similar patterns of fast locomotion, slow locomotion and anterior reaching suggest that, for these motor circuits at least, this is a possibility. Alternatively, it is possible that many of these descending neurons modulate distinct aspects of these motor programs.

Third, another way to generate behavioral complexity is through coding different behaviors via combinations of descending neurons. We examined a few lines that target multiple descending neurons. We compared behaviors produced by these “multi-hit” split-GAL4 lines with lines that targeted the individual neurons and found only weak evidence for the emergence of new behaviors when descending neurons were triggered in combination. For example, both DNa05 and DNd02 produce slightly different phenotypes when activated in combination with DNa07 and DNd03, respectively, as compared to when lines targeting these neurons are activated alone (see Figure S5). However, our collection contains, by design, few lines driving expression in combinations of descending neuron types. Therefore, further exploration of this idea will require the generation and characterization of additional lines.

Finally, descending neurons could be re-used in multiple behavioral contexts. While there are to date no published examples of a single descending neuron triggering different context-dependent behaviors, there are multiple cases in which descending neurons exhibit different physiological responses depending on the state of the animal (e.g. walking, flying, courting, etc.) (Böhm & Schildberger, 1992; B Hedwig, 2000; R.

M. Olberg, 1983; R. Olberg & Willis, 1990; E. M. Staudacher, 2001; E. Staudacher & Schildberger, 1998; Strausfeld & Bassemir, 1985; Zorović & Hedwig, 2011). Our results strongly support a role for context dependency for two reasons. First, the high level of mutual information between behaviors immediately before and after red light activation seen in lines that have multiple red light activated regions indicates that even within the relatively confined system of our assay, the behavior of the fly immediately before descending neuron activation biases the behavioral output in many cases. Second, our observation that substrate specific behaviors, such as foreleg tapping, reaching, and locomotion are strongly represented in our dataset, while flight and courtship behaviors are less prevalent suggests that descending neuron outputs may be context dependent. By forcing the flies to remain on a two dimensional substrate in isolation, we may have observed predominantly indirect results of behaviors that would normally take place in a different context. For example, when we activated a line expressing in DNp01, the giant fiber, a neuron known to elicit a rapid escape response initiated by a jump when optogenetically activated (Lima & Miesenbock, 2005) we detected the flies running after returning back to the ground because the jump was too fast (~30 ms) to be detected in our assay. It is also possible that some of these descending neurons are never naturally activated in the two-dimensional context of walking and that proprioceptive feedback may have generated abnormal behaviors in our assay.

Our objective, quantitative assessment of a descending neuron activation screen provides a foundation for understanding descending neuron functions more broadly. Using similar analytical approaches to study the results of descending neuron activation and inactivation in other behavioral settings in the future will broaden our understanding

of how descending neurons direct motor patterns in specific behavioral contexts and reveal how the fly's rich behavioral repertoire can be encoded with only a few hundred neurons.

Materials and Methods

Fly stocks and fly handling

The descending neuron split-GAL4 driver collection is described in Namiki et al (Namiki et al 2017). Male flies were crossed to virgin females carrying *20xUAS-CsChrimson-mVenus* (Klapoetke et al., 2014b) integrated into the *attP18* landing site (Markstein, Pitsouli, Villalta, Celniker, & Perrimon, 2008) and transferred to Dickson lab power food (1L water, 10g agar, 80g Brewer's yeast, 20g yeast extract, 20g peptone, 30g sucrose, 60g dextrose, 0.5g $\text{MgSO}_4 \cdot 6\text{H}_2\text{O}$, 0.5g $\text{CaCl}_2 \cdot 2\text{H}_2\text{O}$, 6mL propionic acid and 7mL 15% Nipagin). For the initial screen, experimental animals were raised on power food supplemented with 0.2 mM retinal. This concentration was increased to 0.4 mM for animals that were re-assayed at a higher light intensity. All flies (except parental stocks) were handled under 453 nm blue LEDs and reared in dark blue acrylic boxes (acrylic available from McMaster-Carr, # 8505K84) at 22°C on a 12 hour lights on:12 hour lights off day:night cycle. Individual male flies were collected upon eclosion and housed singly in 2mL wells in a 96 well "condo," with power food (with or without retinal) deposited in the bottom of each well, which was sealed at the top with an airpore sheet (Qiagen #195761). Flies were imaged at age 7-12 days, within 4 hours of lights on.

Data Collection

Single flies were loaded into individual trays made from 4.5 mm clear acrylic topped with a fly “bubble” 3 cm in diameter and 4 mm at its tallest point, which was vacuum molded from clear 0.020” PETG thermoform plastic (WidgetWorks, available on Amazon) (Klibaite (2017)). PETG was placed in a frame, heated in a Oster Convection Bake pizza oven set at 350°F until the plastic started to deform (about 20 seconds), then placed on a vacuum manifold. To further encourage the flies to remain on the 2 dimensional acrylic surface, the bubbles were coated with Sigmacote siliconizing reagent one day prior to imaging and lightly wiped with ethanol to remove the excess silicone.

For each descending neuron split-GAL4 line six retinal-fed experimental animals and six non-retinal-fed control animals were imaged simultaneously. For imaging, flies were placed in individual fly bubbles atop custom light tables (3 identical light tables, each imaging 4 flies). These tables consisted of a custom light board topped with a 0.75” 3D printed white plastic standoff that was lined with infrared reflective tape, and which was capped with a diffuser made from 0.125” white plexiglass acrylic (available from eplastics.com, # ACRY24470.125PM24X48), which had 50% light transmittance. The light board itself consisted of an array of 256 IR LEDs (Osram Opto SFH 4050-Z, 850 nm wavelength) arrayed in a 16 x16 pattern, spaced 7.14 mm apart, and 64 red LEDs (Philips Lumileds, LXM2-PD01-0050, 627 nm) arranged in an 8x8 pattern, spaced 14.28 mm apart. IR and red LED intensity was controlled separately by 0-2.5V control voltages, yielding 0-100mA for the IR LEDS and 0-400 mA for the red LEDs. We set the IR LEDs to 1V, which provided even illumination without overheating the flies. We used 0.2V (4.5 mW/cm²) red light in the initial screen and 1.0V (9 mW/cm²) red light when

re-screening a subset of lines. All three light tables were connected to a 68-Pin unshielded I/O connector block (National Instruments, CB-68LP), then to an M Series multifunction DAQ board (National Instruments, NI USB-6281), so that all tables could be run simultaneously from a single computer. Each light table was topped with a 10" square frame constructed from off the shelf parts from Thorlabs, which supported four 1.3 MP grayscale USB cameras (Point Grey FL3-U3-13Y3M-C, 1 camera per fly) on optical rails, whose X/Y/Z coordinates could be adjusted relative to the fly bubble. Each camera was fitted with an HR F2/35mm lens from Thorlabs and an 800 nm longpass filter (Thorlabs, FEL0800). Each set of four cameras was connected to a separate Dell Precision T3600 Tower Workstation. Each was fitted with two 100 GB internal solid state drives, so that 2 cameras wrote to each SSD.

Cameras were programmed using NI-MAX and custom software written in Labview (National Instruments). Data acquisition and the LED light tables were controlled by custom software written in Labview. In brief, a master computer ran a single program that (1) turned the red and infrared (Berman et al., 2014) LEDs on for all three light tables, the former running a program of 15 seconds, then off for 45 seconds, for 30 cycles; (2) started all 12 cameras recording; (3) recorded the position of the fly's centroid for each frame for each camera; and (4) grabbed the frame number for each camera over the network every 2-3 frames, and wrote the frame number and red LED status from the light tables to a single text file. All movies were recorded as uncompressed avi files at 100 frames per second. Each camera was set to 1024 x 1024 pixel resolution that encompassed the entire 3 cm arena. However, flies were tracked

using a blob detector and only a 150x150 pixel box centered on each fly was saved and used for analysis.

Behavior Space Generation

Our approach for generating a behavior space largely follows the methodology originally described in Berman, 2014 (Berman et al., 2014), which describes much of the procedure in additional detail. We first segmented flies using Canny's method for edge detection (Canny, 1986) and morphological dilation to find the outline of the fly. All pixels within the corresponding closed curve were considered part of the fly. We assumed that all flies had identical morphology but variable sizes. We calculated a rescaling factor for each fly by segmenting 100 randomly-selected images from a single fly and finding the pixels belonging to that fly's body (head, thorax, and abdomen) in each of them, ignoring pixels associated with the wings and legs. Body pixels were assigned via a two-component Gaussian mixture model, and the average value of the number of pixels was chosen as the body area. All frames from a single movie were then uniformly re-scaled to make the number of body pixels in the average image equal to that in a reference image of a fly. We then rotationally aligned segmented, recalled images by finding the maximal angular cross-correlation of the magnitudes of the two-dimensional polar Fourier transforms between the image and a reference image. This reference image was common to all aligned images. Translational registration was then performed by maximizing the spatial cross-correlation.

Postural decomposition was performed as described in Berman (2014). Images were Radon-transformed using a 2 degree spacing, and the 9,781 Radon-space pixels that

contained the most variance were kept for further analysis (>95% of the total variance). We then performed principal components analysis (PCA) on these data, keeping the 50 modes capturing the most variance (>90% of the total variance). We projected the segmented and aligned images onto the found eigenvectors to create a set of time series that were representative of the postural movements of the fly. To obtain dynamic information about these time series, we applied a Morlet continuous wavelet transform to these time series. We transformed each mode separately, using 25 frequency channels that were dyadically spaced between 1 Hz and 50 Hz, retaining only the amplitudes of the resulting complex numbers.

Low dimensional embedding of these wavelet time series using t-Distributed Stochastic Neighbor Embedding (t-SNE) (van der Maaten & Hinton, 2008) largely followed the approach in (Berman et al., 2014) as well. A distance metric between points in time was calculated via the the Kullback-Leibler divergence (Cover & Thomas, 2005) between their associated normalized mode-frequency spectra. Because this data set contains several orders of magnitude more data than can be calculated through brute-force minimization of the t-SNE cost function, we used the sub-sampling technique described in (Berman et al., 2014) to identify 600 representative data points from each of the recording sessions. From here, points were randomly assigned subsequent groupings such that each of these groups contained 36,000 data points. The same sub-sampling process was performed amongst these data points, but now keeping twice as many data points as in the previous iteration. This process was repeated until a data set of 36,000 points was obtained. We minimized t-SNE for this data set to create a low-dimensional embedding. We used the re-embedding procedure described in (Berman et al., 2014) to

include data from outside the 36,000-point training set into the embedding, resulting in the overall density seen in Figure 1.

Statistical Analysis

Our main goal for the statistical analysis of the behavior space data was to isolate regions of the map that were significantly affected by optogenetic stimulation. Here, we assessed significance by (1) comparing the flies' behavior when the LED was on versus when the LED was off, and (2) requiring that the effect of the LED stimulation be larger in the experimental flies than in the control flies. Specifically, we compared the flies' behavior during the first three seconds of stimulation ($t=0s$ to $t=3s$, where the LED turns on at $t=0$) to their behavior between stimulation ($t=30s$ to $t=45s$). To statistically assess whether a particular region of the behavior space was significantly affected by the stimulus, we first defined $\rho_{i,n}^{on}(x,y)$ to be the average behavior space density for fly i during the n th cycle at location (x,y) during the first 3 seconds of excitation and $\rho_{i,n}^{off}(x,y)$ to be the same, but during the 15s window furthest from the stimulation. We then tested whether $\rho_{i,n}^{on}(x,y)$ was significantly different from $\rho_{i,n}^{off}(x,y)$ through a Wilcoxon rank sum test with Šidák corrections ($p < .05$ after corrections) (Šidák, 1967). To calculate the number of corrections, we conservatively assumed that the number of measurements was equal to 2^H , where H was the entropy of the mean density of the behavior space. This is likely an over-estimate of the number of comparisons, but it provides an upper-bound for the number of distinctions that could be made.

To compare the effect of the optogenetic stimulus on the experimental flies to that of the effect on the control flies, we computed the quantity $\chi_{i,n}(x,y) = \rho_{i,n}^{on}(x,y) -$

$\frac{1}{2}(\rho_{i,n-1}^{off}(x,y) + \rho_{i,n}^{off}(x,y))$, which was the behavior space density during light stimulation compared to the average of the two preceding time periods with no light stimulation. We thus assessed statistical significance by using a Wilcoxon rank sum test with Šidák corrections ($p < .05$ after corrections) to compare $\{\chi_{i,n}(x,y)\}_{i \in \text{experimental flies}}$ with $\{\chi_{i,n}(x,y)\}_{i \in \text{control flies}}$. For a point, (x,y) , in the behavior space to be considered significantly affected by the stimulus, we required that both of these tests—within experimental flies test and experimental versus control flies test—yielded a significant result.

Behavior activation maps for individual descending interneurons (Figure 6) were calculated by averaging together the maps of significantly significant activations ($E[\chi_{i,n}(x,y)]_{i,n} > 0$) from each of the lines exciting that neuron.

Stimulation-response entropy curves (Figure 2A & D) were generated by first aligning each time point to its associated phase within the 60 second LED on-off cycle. For each phase within the cycle, we found all embedding points from all relevant trials that were detected within ± 200 ms (using periodic boundary conditions). We then generated a histogram of these points, normalized and convolved the resulting values with a symmetric two-dimensional Gaussian of width $\sigma = 2$, to generate a probability density function, $p_t(x,y)$. From this, the entropy curve value at phase t was given by $H(t) = \int dx dy p_t(x,y) \log p_t(x,y)$. We then pooled data from all individuals of a specific type together (i.e. all control flies from a given line or all experimental flies from a given line) to calculate these curves.

Mutual information between pre-stimulus behavior space densities and post-stimulus regions was computed by numerically integrating the integral:

$MI(\rho_{pre}; R_{post}) = \sum_{k=0}^m \int d\vec{x} p_{pre}(\vec{x}|R_k) \log_2 \frac{p_{pre}(\vec{x}|R_k)}{\sum_{\ell=0}^m p_{pre}(\vec{x}|R_\ell)p(R_\ell)},$ where $p_{pre}(\vec{x}|R_k)$ is
 the conditional probability of observing the fly's behavior to be at location \vec{x} between 1.5
 and 0.5 seconds before the stimulus onset and $p(R_k)$ is the probability that the fly
 transitions to region R_k following the stimulus onset. Finite data-size corrections were
 performed by drawing subsets of the data with replacement and extrapolating to an
 infinite number of trials, and error bars were generated by extrapolating the calculated
 variance in a similar manner (Bialek, 2012). The region of transition for each trial was
 assigned by finding the mode of the behavior space distribution during the first second
 subsequent to the onset of the stimulus. If the location of the mode of the distribution for
 that trial was within or closer than 5-pixels to the edge of a region, it was assigned to that
 region, unless another region was closer. Trials not assigned to any of the regions were
 given a "zero" label, as reflected in the previous equation.

To provide a sense of scale, if there are N significantly activated regions, the
 maximum possible mutual information one could potentially measure between the prior
 distribution and the activated region would be $\log_2(N)$ bits. Note, however, that we
 assigned an additional state corresponding to the fly performing a behavior outside of the
 significantly activated regions subsequent to the light turning on, thus making the
 maximal possible mutual information $\log_2(N + 1)$. This additional "zero" state is
 necessary to account for the possibility that the significant regions might be exhibited
 only in a context-dependent manner, leading to no significant phenotype when the fly is
 performing some behaviors at the onset of red light stimulation and leading to a
 phenotype if other actions are being exhibited.

612

613 **Acknowledgements**

614 We thank Vivek Jayaraman for reagents and feedback, Jan Ache and Ugne Klibaite for
 615 discussions, Todd Lavery and members of the Janelia Fly Core for their support, and
 616 Steven Sawtelle, Igor Negroshov, Ben Arthur and Roger Rogers for help with the rig, fly
 617 bubble design and fabrication. The driver lines were developed as part of the Descending
 618 Interneuron Project Team at the Janelia Research Campus. This project was supported by
 619 the Janelia Research Campus Visitor Program and NIH GM098090.

620

621 **References**

622 Alivisatos, A. P., Chun, M., Church, G. M., Greenspan, R. J., Roukes, M. L., & Yuste, R.
 623 (2012). The brain activity map project and the challenge of functional connectomics.
 624 *Neuron*, 74(6), 970–4. <http://doi.org/10.1016/j.neuron.2012.06.006>
 625 Bentley, D. (1977). Control of cricket song patterns by descending interneurons. *Journal*
 626 *of Comparative Physiology*, 116(1), 19–38. <http://doi.org/10.1007/BF00605514>
 627 Berman, G. J., Choi, D. M., Bialek, W., & Shaevitz, J. W. (2014). Mapping the
 628 stereotyped behaviour of freely moving fruit flies. *Journal of the Royal Society,*
 629 *Interface*, 11(99), 20140672. <http://doi.org/10.1098/rsif.2014.0672>
 630 Bialek, W. (2012). *Biophysics: searching for principles*. Princeton: Princeton University
 631 Press.
 632 Bidaye, S. S., Machacek, C., Wu, Y., & Dickson, B. J. (2014). Neuronal control of
 633 *Drosophila* walking direction. *Science*, 344(6179), 97–101.
 634 <http://doi.org/10.1126/science.1249964>

635 Böhm, H., & Schildberger, K. (1992). Brain Neurones Involved in the Control of
636 Walking in the Cricket *Gryllus Bimaculatus*. *Journal of Experimental Biology*.

637 Canny, J. (1986). A Computational Approach to Edge Detection. *IEEE Transactions on*
638 *Pattern Analysis and Machine Intelligence*, PAMI-8(6), 679–698.
639 <http://doi.org/10.1109/TPAMI.1986.4767851>

640 Cover, T. M., & Thomas, J. A. (2005). *Elements of Information Theory*. *Elements of*
641 *Information Theory*. <http://doi.org/10.1002/047174882X>

642 Gras, H., & Kohstall, D. (1998). Current injection into interneurons of the terminal
643 ganglion modifies turning behaviour of walking crickets. *Journal of Comparative*
644 *Physiology. A, Neuroethology, Sensory, Neural, and Behavioral Physiology*, 182(3),
645 351–361.

646 Griss, C., & Rowell, C. H. F. (1986). Three descending interneurons reporting deviation
647 from course in the locust. *Journal of Comparative Physiology. A, Neuroethology*,
648 *Sensory, Neural, and Behavioral Physiology*, 158(6), 765–774.

649 Gronenberg, W., & Strausfeld, N. J. (1990). Descending neurons supplying the neck and
650 flight motor of Diptera: physiological and anatomical characteristics. *The Journal of*
651 *Comparative Neurology*, 302(4), 973–991.

652 Hedwig, B. (1994). A cephalothoracic command system controls stridulation in the
653 acridid grasshopper *Omocestus viridulus* L. *J Neurophysiol*, 72(4), 2015–2025.

654 Hedwig, B. (2000). Control of Cricket Stridulation by a Command Neuron: Efficacy
655 Depends on the Behavioral State. *J Neurophysiol*, 83(2), 712–22.

656 Heinrich, R. (2002). Impact of descending brain neurons on the control of stridulation,
657 walking, and flight in orthoptera. *Microscopy Research and Technique*, 56(4), 292–

658 301.

659 Hensler, K. (1992). Neuronal co-processing of course deviation and head movements in
660 locusts. *Journal of Comparative Physiology. A, Neuroethology, Sensory, Neural,*
661 *and Behavioral Physiology*, 171(2), 257–271.

662 Hsu, C. T., & Bhandawat, V. (2016). Organization of descending neurons in *Drosophila*
663 melanogaster. *Scientific Reports*, 6, 20259. <http://doi.org/10.1038/srep20259>

664 Kanzaki, R., Ikeda, A., & Shibuya, T. (1994). Morphological and physiological
665 properties of pheromone-triggered flipflopping descending interneurons of the male
666 silkworm moth, *Bombyx mori*. *Journal of Comparative Physiology. A,*
667 *Neuroethology, Sensory, Neural, and Behavioral Physiology*, 175(1), 1–14.

668 Kien, J. (1983). The Initiation and Maintenance of Walking in the Locust: An Alternative
669 to the Command Concept. *Proceedings of the Royal Society B: Biological Sciences*,
670 219(1215), 137–174. <http://doi.org/10.1098/rspb.1983.0065>

671 Kien, J. (1990). Neuronal activity during spontaneous walking--I. Starting and stopping.
672 *Comparative Biochemistry and Physiology. A, Comparative Physiology*, 95(4), 607–
673 621.

674 King, D. G., & Wyman, R. J. (1980). Anatomy of the giant fibre pathway in *Drosophila*.
675 I. Three thoracic components of the pathway. *Journal of Neurocytology*, 9(6), 753–
676 770. <http://doi.org/10.1007/BF01205017>

677 Klapoetke, N. C., Murata, Y., Kim, S. S., Pulver, S. R., Birdsey-Benson, A., Cho, Y. K.,
678 ... Boyden, E. S. (2014b). Independent optical excitation of distinct neural
679 populations. *Nature Methods*, 11(3), 338–46. <http://doi.org/10.1038/nmeth.2836>

- 680 Klibaite, U., Berman, G. J., Cande, J., Stern, D. L., & Shaevitz, J. W. (2017). An
681 unsupervised method for quantifying the behavior of paired animals. *Physical*
682 *Biology*, 14(1), 015006. <http://doi.org/10.1088/1478-3975/aa5c50>
- 683 Larimer, J. L. (1988). The command hypothesis: a new view using an old example.
684 *Trends in Neurosciences*, 11(11), 506–510. <http://doi.org/10.1016/0166->
685 2236(88)90013-6
- 686 Lima, S. Q. & Miesenböck, G. (2005). Remote control of behavior through genetically
687 targeted photostimulation of neurons. *Cell*, 121(1), 141-152.
688 <http://doi.org/10.1016/j.cell.2005.02.004>
- 689 Marder, E. & Goaillard, J.-M. (2006). Variability, compensation and homeostasis in
690 neuron and network function. *Nature Review Neuroscience*, 7, 563-574.
691 <http://doi.org/10.1038/nrn1949>
- 692 Markstein, M., Pitsouli, C., Villalta, C., Celniker, S. E., & Perrimon, N. (2008).
693 Exploiting position effects and the gypsy retrovirus insulator to engineer precisely
694 expressed transgenes. *Nature Genetics*, 40(4), 476–83. <http://doi.org/10.1038/ng.101>
- 695 Milde, J. Igen J., & Strausfeld, N. J. (1990). Cluster organization and response
696 characteristics of the giant fiber pathway of the blowfly *Calliphora erythrocephala*.
697 *The Journal of Comparative Neurology*, 294(1), 59–75.
698 <http://doi.wiley.com/10.1002/cne.902940106>
- 699 Namiki, S., Dickinson, M.H., Wong, A.M., Korff, W., and Card, G.M. (2017) The
700 functional organization of descending sensory-motor pathways in *Drosophila*.
701 *bioRxiv*.
- 702 Okada, R., Sakura, M., & Mizunami, M. (2003). Distribution of dendrites of descending

neurons and its implications for the basic organization of the cockroach brain. *The Journal of Comparative Neurology*, 458(2), 158–174.

Olberg, R. M. (1983). Pheromone-triggered flip-flopping interneurons in the ventral nerve cord of the silkworm moth, *Bombyx mori*. *Journal of Comparative Physiology A*, 152(3), 297–307. <http://doi.org/10.1007/BF00606236>

Olberg, R., & Willis, M. (1990). Pheromone-modulated optomotor response in male gypsy moths, *Lymantria dispar* L.: Directionally selective visual interneurons in the ventral nerve cord. *Journal of Comparative Physiology A*, 167(5). <http://doi.org/10.1007/BF00192665>

Pfeiffer, B. D., Ngo, T.-T. B., Hibbard, K. L., Murphy, C., Jenett, A., Truman, J. W., & Rubin, G. M. (2010). Refinement of tools for targeted gene expression in *Drosophila*. *Genetics*, 186(2), 735–755.

Ritzmann, R. E., & Büschges, A. (2007). Adaptive motor behavior in insects. *Current Opinion in Neurobiology*, 17, 629–636. <http://doi.org/10.1016/j.conb.2008.01.001>

Rowell, C. H., & Reichert, H. (1986). Three descending interneurons reporting deviation from course in the locust. II. Physiology. *Journal of Comparative Physiology. A, Sensory, Neural, and Behavioral Physiology*, 158(6), 775–94.

Šidák, Z. (1967). Rectangular Confidence Regions for the Means of Multivariate Normal Distributions. *Journal of the American Statistical Association*, 62(318), 626–633. <http://doi.org/10.1080/01621459.1967.10482935>

Simon, J. C., & Dickinson, M. H. (2010). A new chamber for studying the behavior of *Drosophila*. *PLoS ONE*, 5(1), e8793.

Staudacher, E. (1998). Distribution and morphology of descending brain neurons in the

726 cricket gryllus bimaculatus. *Cell and Tissue Research*, 294(1), 187–202.

727 Staudacher, E. M. (2001). Sensory responses of descending brain neurons in the walking

728 cricket, *Gryllus bimaculatus*. *Journal of Comparative Physiology. A*, 187(1), 1–17.

729 Staudacher, E. & Schildberger, K. (1998). Gating of sensory responses of descending

730 brain neurones during walking in crickets. *Journal of Experimental Biology*.

731 Stockinger, P., Kvitsiani, D., Rotkopf, S., Tirián, L., & Dickson, B. J. (2005). Neural

732 circuitry that governs *Drosophila* male courtship behavior. *Cell*, 121(5), 795–807.

733 Strausfeld, N. J., & Bassemir, U. K. (1985). Lobula plate and ocellar interneurons

734 converge onto a cluster of descending neurons leading to neck and leg motor

735 neuropil in *Calliphora erythrocephala*. *Cell and Tissue Research*, 240(3), 617–640.

736 <http://doi.org/10.1007/BF00216351>

737 Strausfeld, N. J., Bassemir, U., Singh, R. N., & Bacon, J. P. (1984). Organizational

738 principles of outputs from Dipteran brains. *Journal of Insect Physiology*, 30(1), 73-

739 96. [https://doi.org/10.1016/0022-1910\(84\)90109-4](https://doi.org/10.1016/0022-1910(84)90109-4)

740 Strausfeld, N. J., & Gronenberg, W. (1990). Descending neurons supplying the neck and

741 flight motor of Diptera: organization and neuroanatomical relationships with visual

742 pathways. *The Journal of Comparative Neurology*, 302(4), 954–972.

743 van der Maaten, L., & Hinton, G. (2008). Visualizing Data using t-SNE. *Journal of*

744 *Machine Learning Research*, 9, 2579–2605.

745 von Philipsborn, A. C., Liu, T., Yu, J. Y., Masser, C., Bidaye, S. S., & Dickson, B. J.

746 (2011a). Neuronal control of *Drosophila* courtship song. *Neuron*, 69(3), 509–522.

747 von Philipsborn, A. C., Liu, T., Yu, J. Y., Masser, C., Bidaye, S. S., & Dickson, B. J.

748 (2011b). Neuronal control of *Drosophila* courtship song. *Neuron*, 69(3), 509–22.

749 <http://doi.org/10.1016/j.neuron.2011.01.011>

750 von Reyn, C. R., Breads, P., Peek, M. Y., Zheng, G. Z., Williamson, W. R., Yee, A. L.,

751 ... Card, G. M. (2014). A spike-timing mechanism for action selection. *Nature*

752 *Neuroscience*, 17(7), 962–970.

753 Zorović, M., & Hedwig, B. (2011). Processing of species-specific auditory patterns in the

754 cricket brain by ascending, local, and descending neurons during standing and

755 walking. *Journal of Neurophysiology*, 105(5), 2181–94.

756 <http://doi.org/10.1152/jn.00416.2010>

757

758

Figures and Figure Legends

Figure 1.

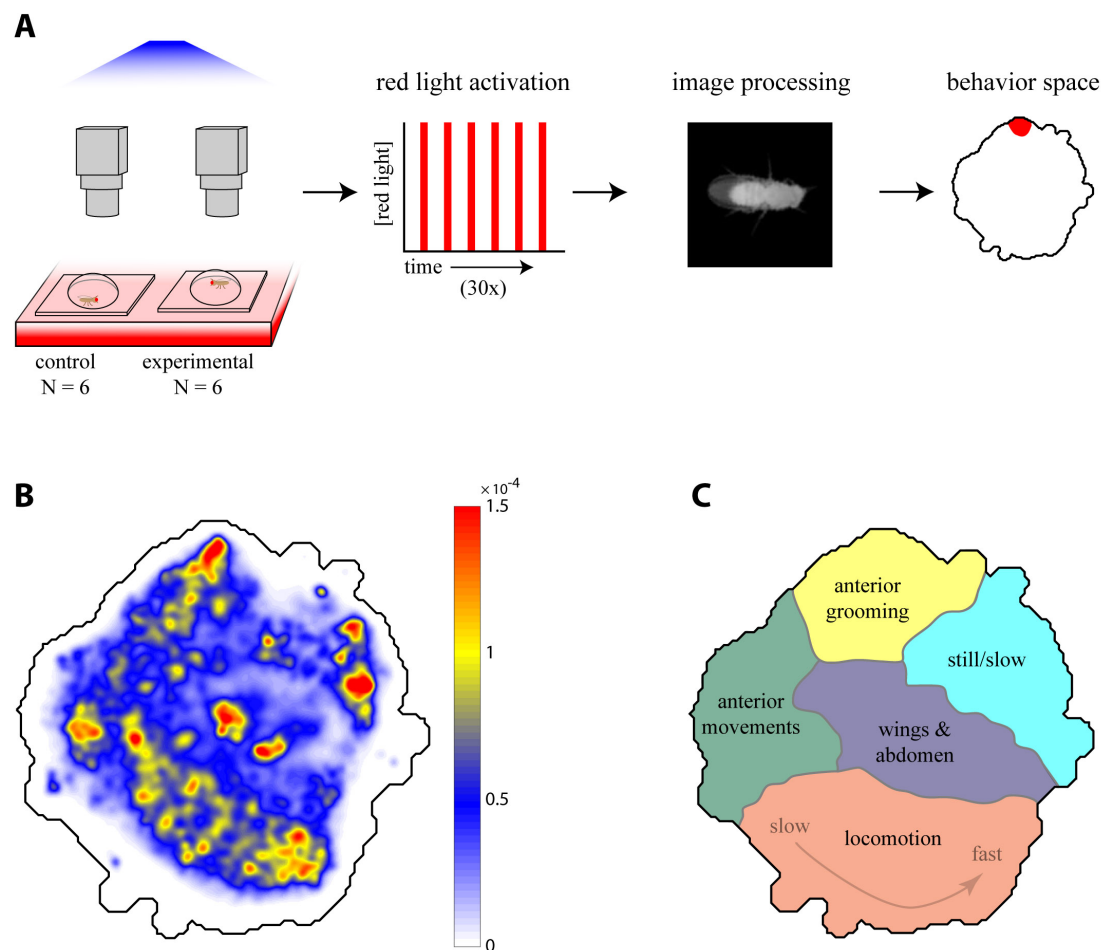
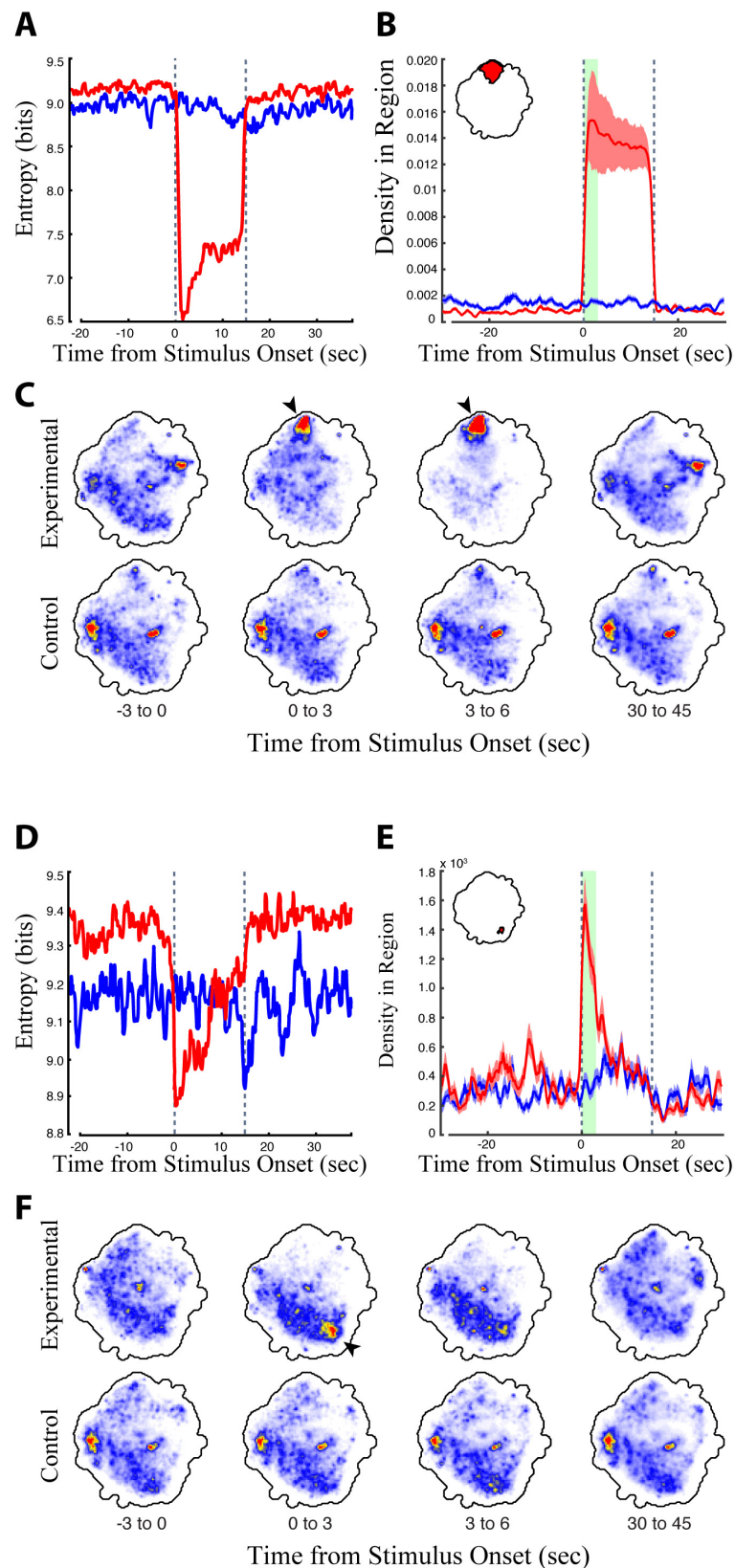


Figure 1. Descending neuron phenotyping pipeline and behavior space. (A) The red light activation rig. Six no retinal control flies and six retinal fed experimental flies were mounted in parallel in individual 3 cm diameter plexiglass bubbles on top of three custom light boards with constant 850 nm infrared light and variable 617 nm red light. The red LEDs were repeatedly turned off and on for 45 sec and 15 sec, respectively. Each fly was

filmed at 150x150 pixel, 100 fps resolution by a single camera. Video data was then aligned and processed, and the line was characterized for its occupancy in the descending neuron behavior space with respect to red light activation and controls. (B) A 2D representation of behaviors in the descending neuron video dataset was generated by applying a probability density function to all the embedded data points (scale bar), which was then convolved with a Gaussian ($\sigma = 1.5$) (C) Localization of various behaviors within the descending neuron behavior space seen in (B), based on human curation of watershedded regions in the space (Supplemental Figure 2, Supplemental movies S1-S6).

779 Figure 2.



780

Figure 2. Analysis of the head grooming DN_g07 & DN_g08 line (SS02635) and the transient fast-running DN_g25 line (SS01602). (A, D) Digital entropy of the distribution of the retinal fed experimental flies (red) and non-retinal fed control flies (blue) in the behavior space relative to the timing of red light stimulus onset (red light turned on at $t = 0$ sec, the time of red light activation is indicated by dashed lines). Experimental flies experience a decrease in entropy when they perform a specific set of behaviors, because they shift from the full range of normal fly behaviors to a subset of red light-activated behaviors. (B, E) Average density \pm the standard deviation in the head grooming map region indicated in red (inset, upper right) in experimental flies (red) and controls (blue) relative to red light activation. The head grooming region was calculated as the region in the map that experienced a statistically significant shift in density in experimental flies but not controls when comparing the first 3 seconds (green bar) of the activation period to the last 15 seconds of the recovery period (Wilcoxon rank sum test, $p < 0.05$, using the Dunn–Šidák correction for multiple hypotheses). (C, F) Average density in the map over a series of 3 second windows (calculated from 6 animals, 30 trials each). Red and blue indicate regions of high and low density, respectively.

Figure 3.

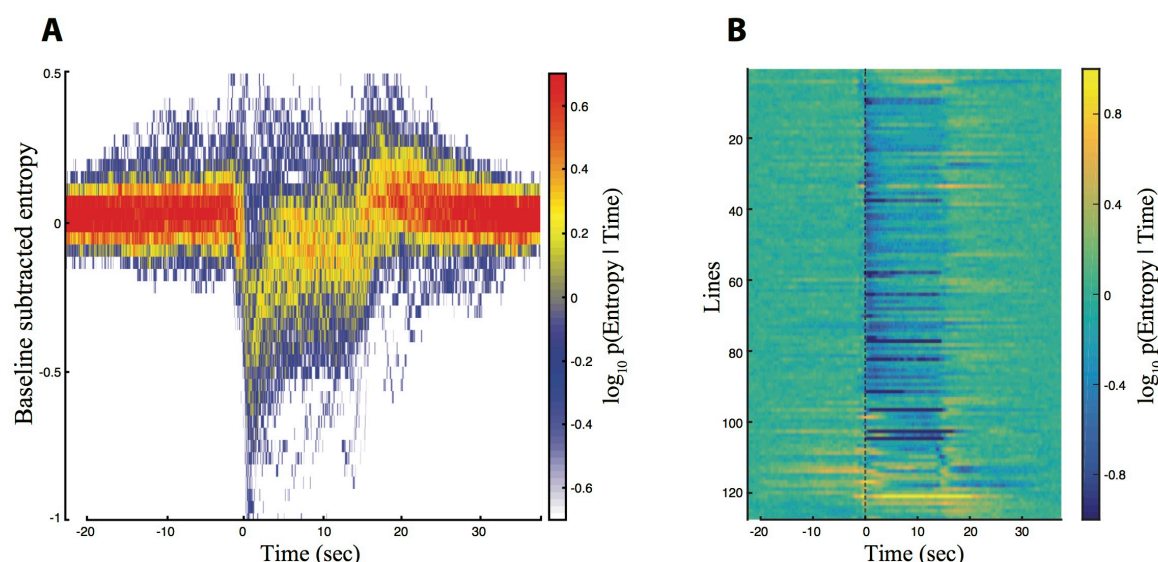
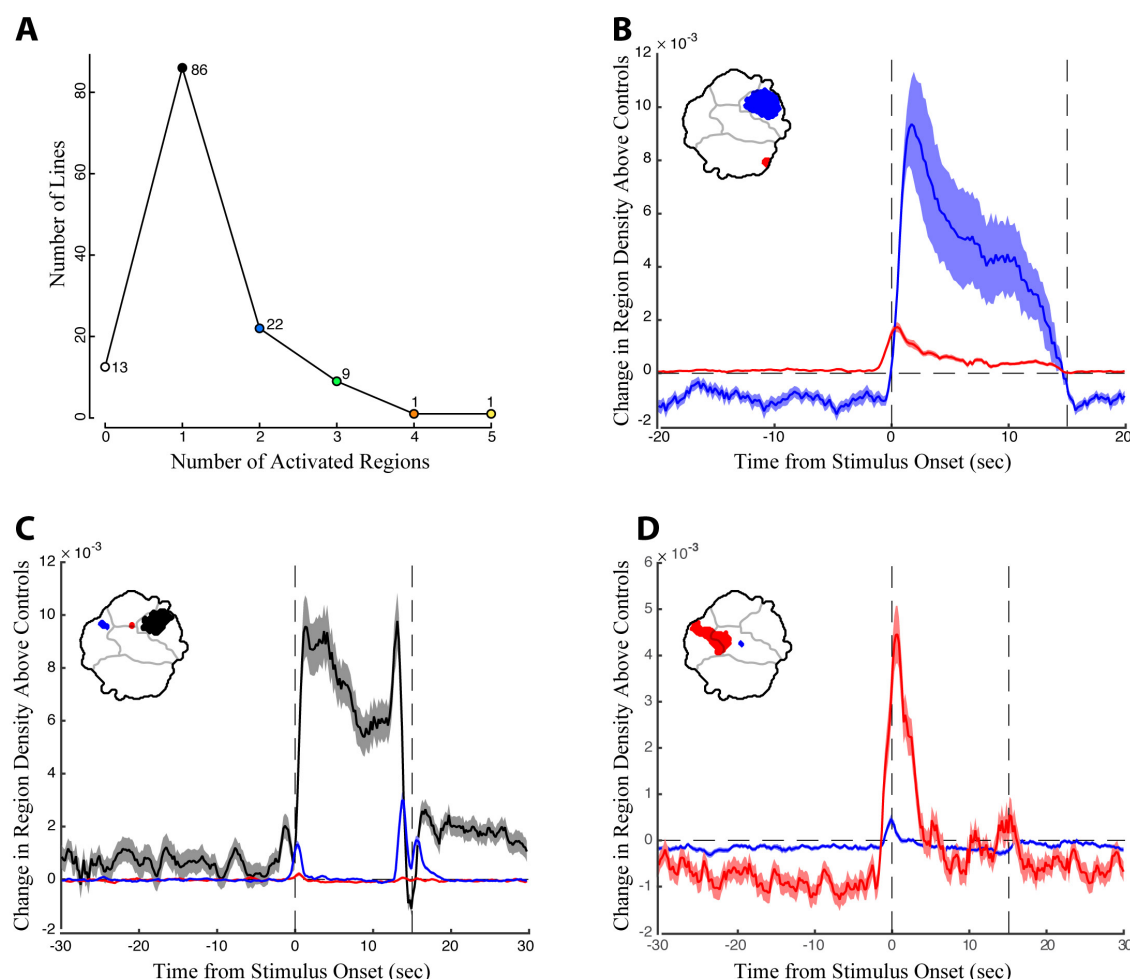


Figure 3. Entropy for all of of descending neuron split-GAL4 lines. Trials were aligned such that the onset of red light activation occurred at $t = 0$ sec (A, B). The red light was turned off at $t = 15$ sec. (A) Baseline subtracted entropy (Y-axis) versus time (X-axis) for all experimental animals and all trials. Colors indicate a probability distribution describing the entropy of experimental animals at a given time in the trial. (B) Entropy levels of experimental animals over the course of the aligned trials (X-axis) shown by line (Y-axis). Warm and blue colors indicate high and low entropy, respectively.

814 Figure 4



815

816 Figure 4. The timing of density shifts in descending neuron lines that occupy multiple
817 behavior space regions. (A) Most lines (86) increase density in only one region of the
818 behavior space upon red light activation. However, some lines occupy multiple regions in
819 the behavior space (B-D) Examples of lines that occupy multiple discontinuous regions
820 upon red light activation. Time is indicated on the X-axis, with the red light turned on at
821 $T = 0$ sec and off at 15 sec. Change in density in the color coded regions in the
822 experimental animals above the controls is indicated on the Y-axis. (B) Line SS01540
823 targeting descending neuron DNp09; (C) SS02542 targeting descending neuron DNb01;
824 (D) SS01049 targeting descending neuron DNp10.

Figure 5.

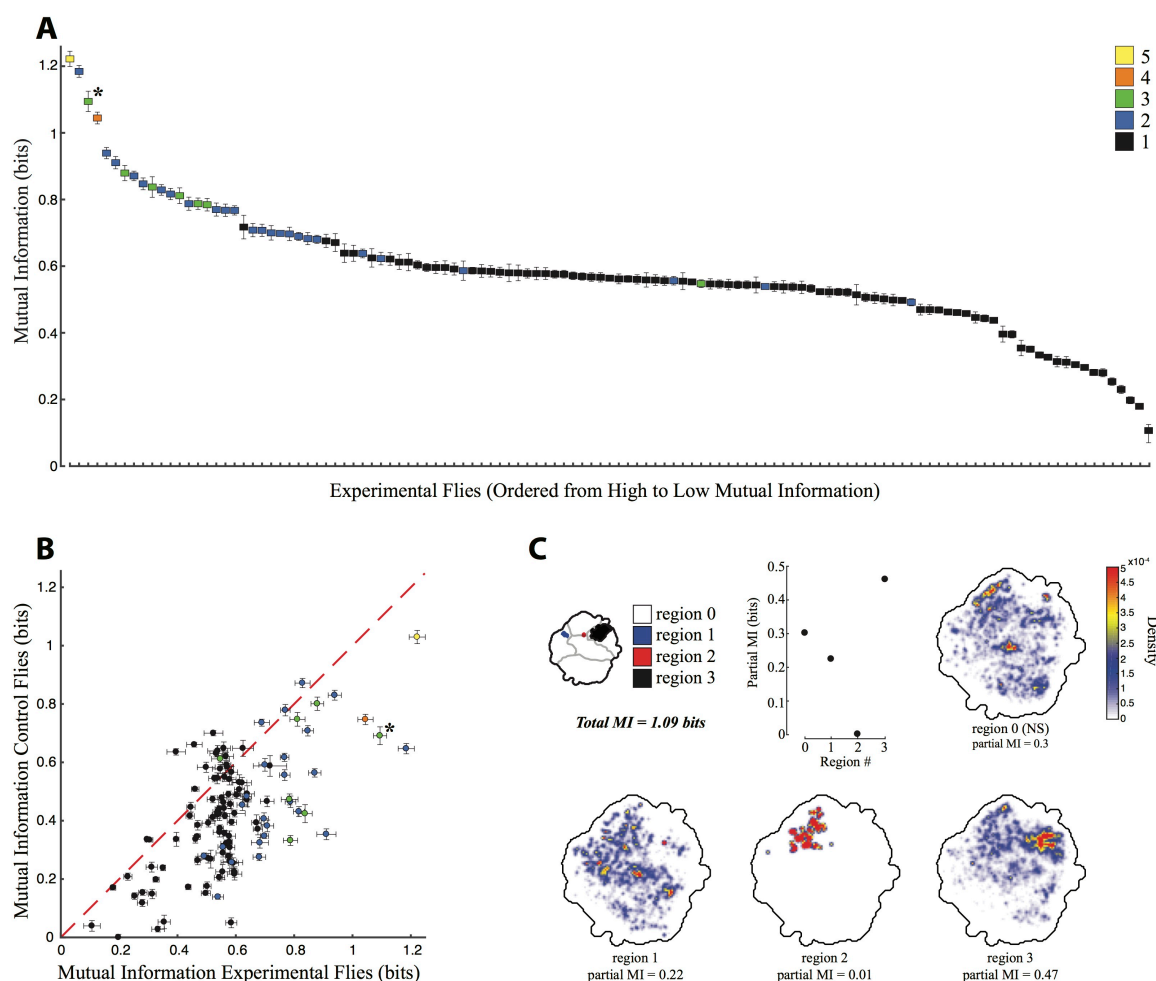
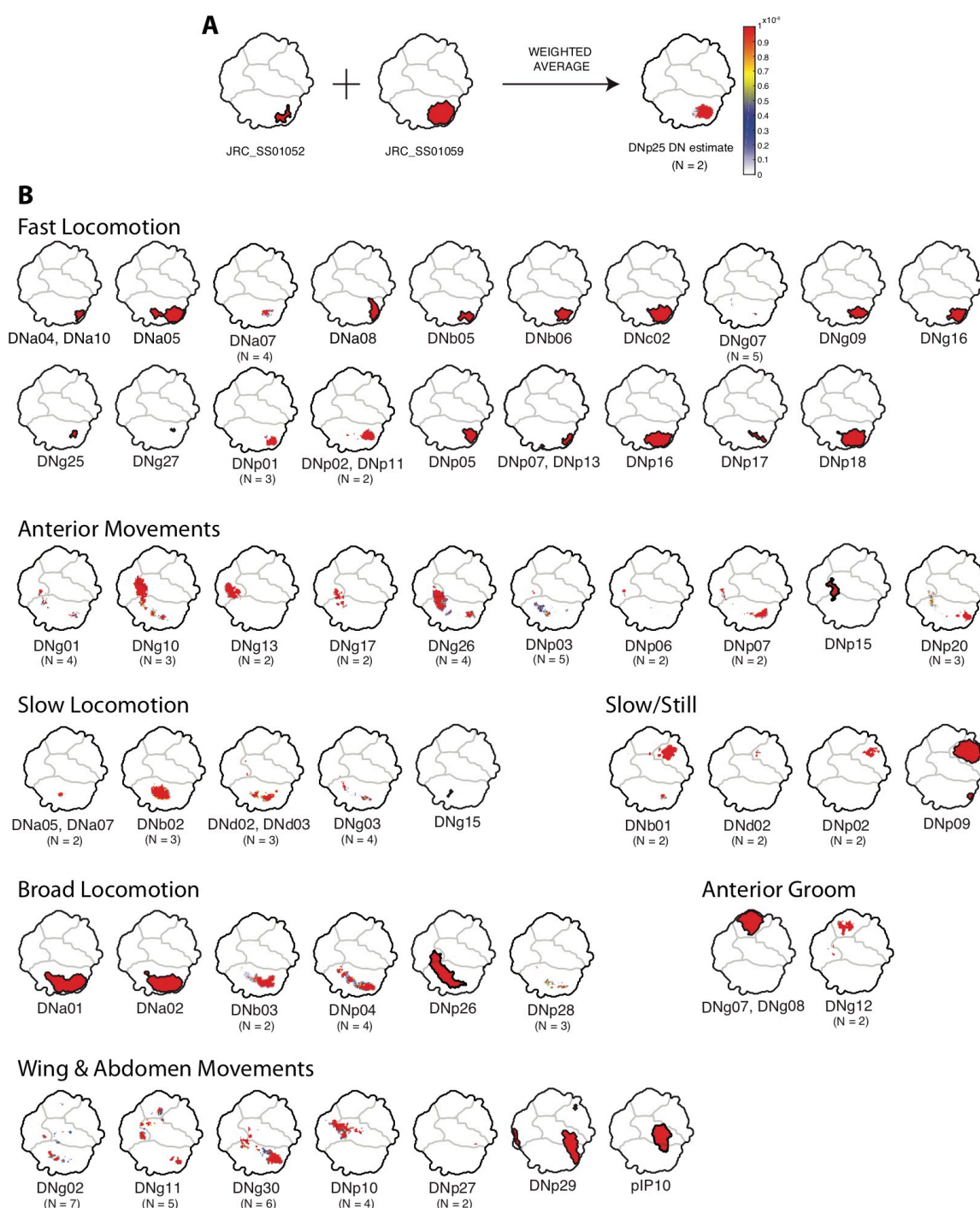


Figure 5. Mutual information between behaviors performed before and during red-light activation. (A) Mutual information for experimental flies, calculated using the density of the flies in the behavior space at $t = -1.5$ to -0.5 seconds prior to red light activation versus density at $t = 0$ to 1.0 seconds after red light activation. Y-axis indicates the mutual information, X-axis is all the lines in order of most to least mutual information, error bars indicate the standard deviation. Lines are color coded by the number of significant regions produced by red light activation, the key is indicated in the upper right, line SS02542 is indicated by an asterisk. (B) Mutual information of experimental flies (X-axis) plotted against that of non-retinal fed control flies (Y-axis), with the same color

836 coding as (A). (C) Partial mutual information for SS02542, showing the density at $t = -$
 837 1.5 to 0.5 that has mutual information with the different regions of the behavior space
 838 after red light activation indicated in the key in the upper left portion of the figure.

839 Figure 6.



840

841 Figure 6. Averages of representative lines for individual descending neurons. Descending
842 neurons are organized according to the region of the behavior space that they activate
843 (Figure 1). (A) Example illustrating the averaging of two lines to produce an estimated

phenotype. Colors indicate the degree to which particular regions are represented in the average. Red regions are highly represented, blue less so, and white not at all. (B) Phenotypes for 53 of the 58 descending neurons in the collection, plus pIP10 (von Philipsborn et al., 2011b). Some descending neurons are represented by a single clean line, others by averaging multiple clean lines. For averages, the number of lines are indicated under the descending neuron name.

Supplementary Information

Figure S1.

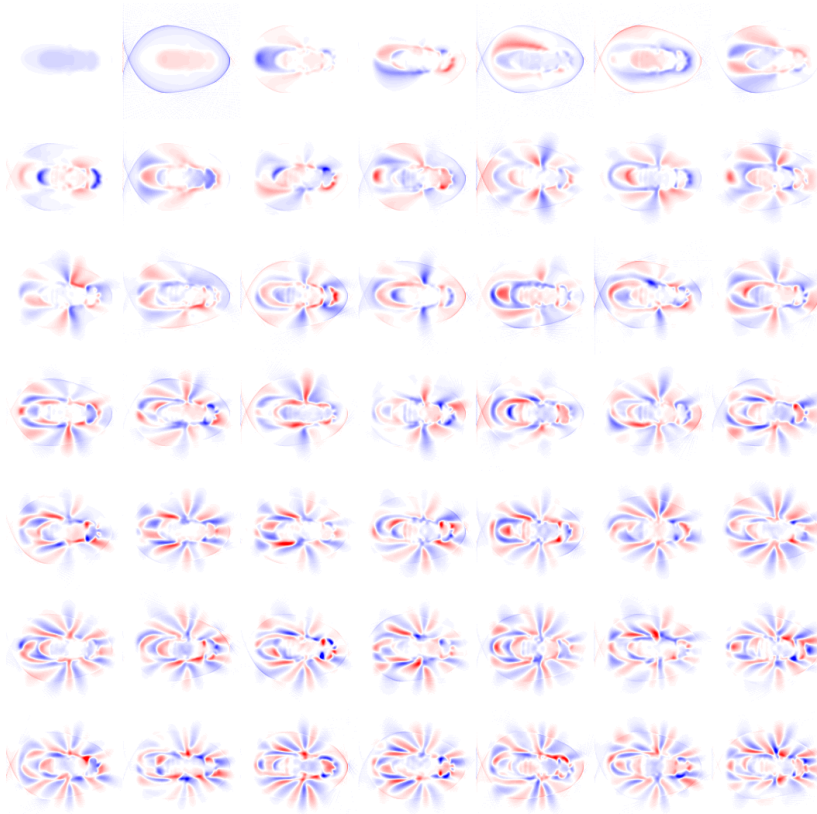


Figure S1. Postural eigenmodes used to build the descending neuron behavior space (Figure 1B).

Figure S2.

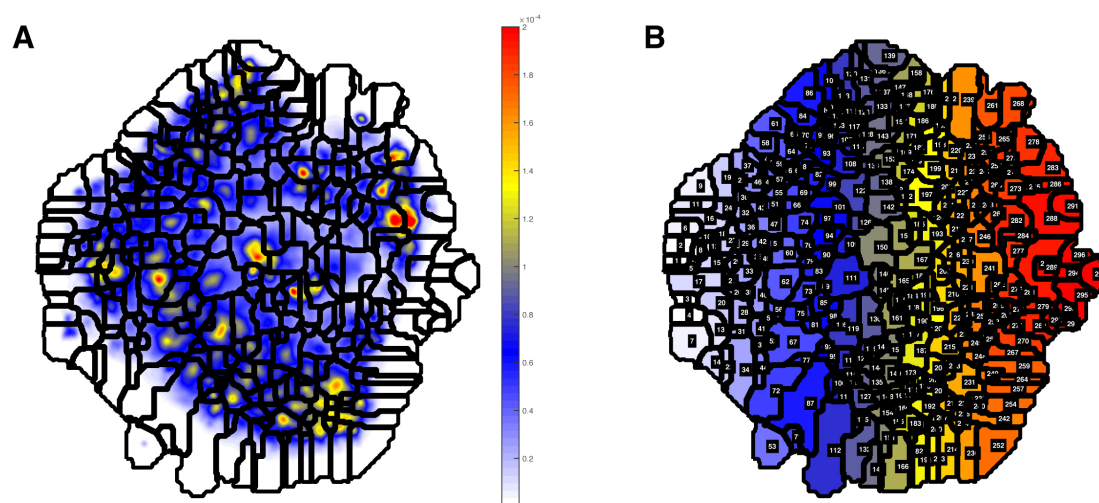
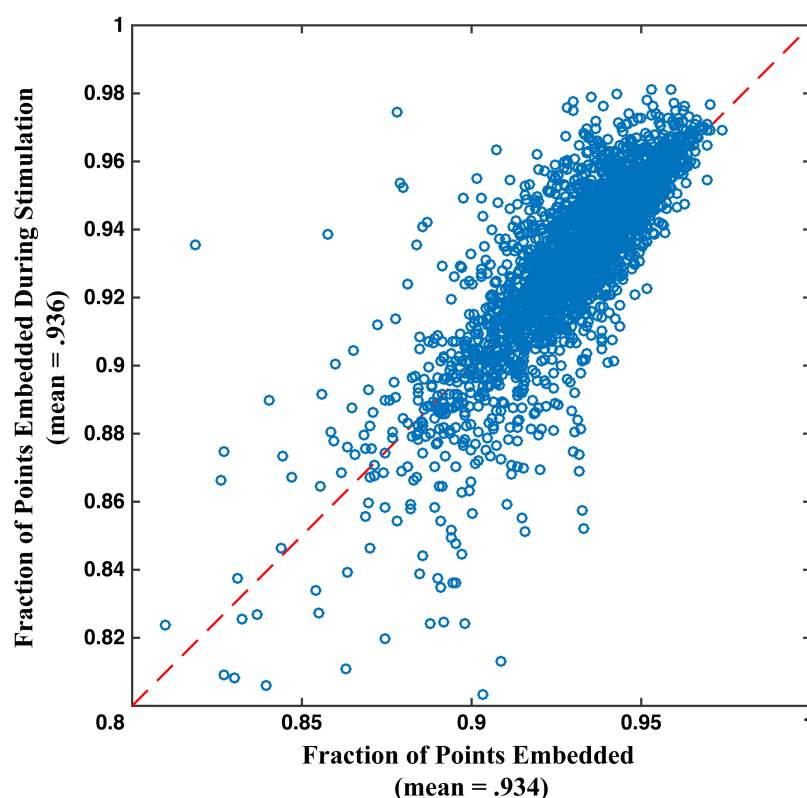


Figure S2. Watershedded regions in the descending neuron behavior space. (A) A watershedding algorithm was used on the behavior space in Figure 1B to identify local density maxima, which represent stereotyped behaviors. (B) Numbered watershedded regions. These correspond to videos underlying all the watershedded regions (Movies S1...S6) which were examined to create the human curated version of the behavior space in Figure 1C.

873 Figure

S3.



874

875 Figure S3. Fraction of video data points for each movie embedded in the behavior space,
 876 during the red light stimulus window (Y axis) and during the recovery period (X axis).
 877 For most movies, between 90 – 95% of frames embedded, with very little difference
 878 between when the red light is on and when the red light is off, indicating that
 879 CsChrimson and red light induced behaviors are well represented in the behavior space.
 880 Failure to embed is usually indicative of imaging flaws, for example when part of the fly
 881 is out of the field of view of the camera.

882

Figure S4.

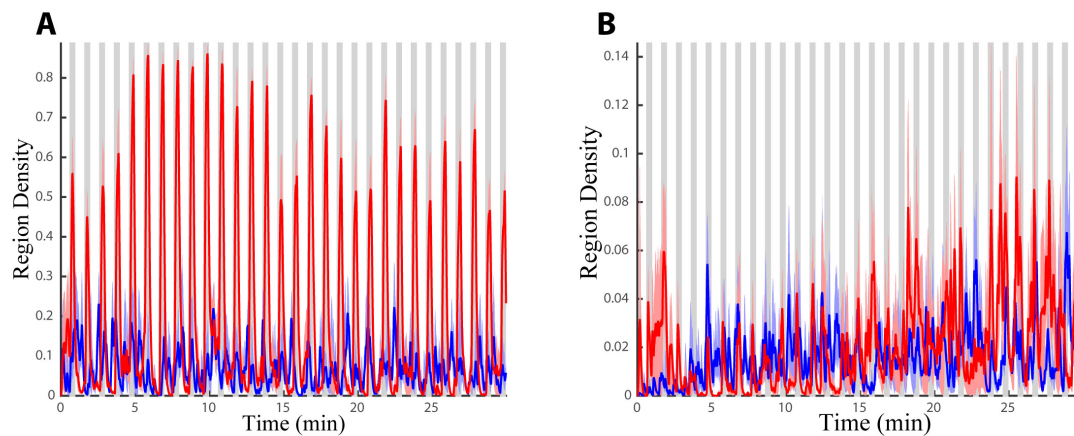


Figure S4. Density in experimental (red) and control (blue) animals in the regions defined in Figure 2A and 2D (A and B, this figure, respectively). Densities shown in Fig. 2B and 2E were averaged for six animals over 30 minutes. Gray bars indicate periods of red light activation.

901
902 Figure S5. Analysis of all the descending neuron split-GAL4 lines. The line by line
903 analysis shown here follows the model of the selected examples described in Figure 2 of
904 the main text.

905

906 *Available at:* http://www.biology.emory.edu/Berman/files/FigureS5_Cande_et_al.pdf

907 (Large file size)

908

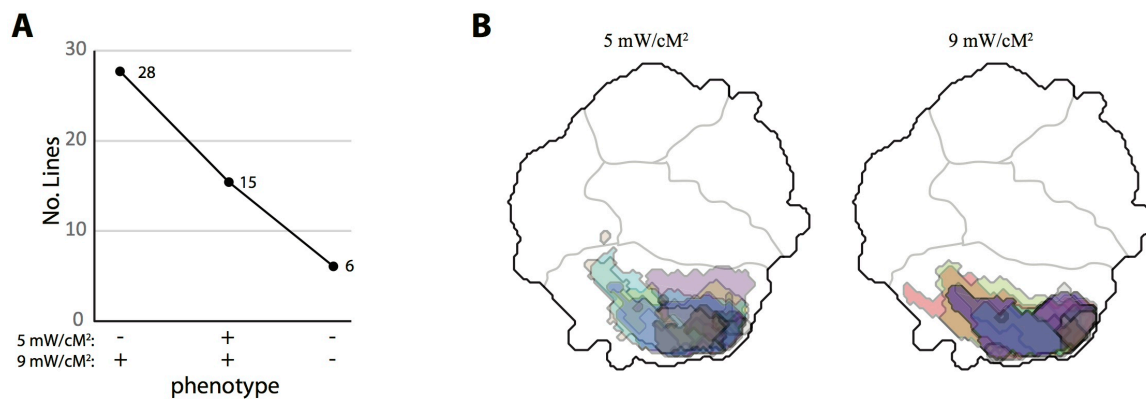


Figure S6. Choosing the red light intensity levels. (A) While most lines were screened at 5 mW/cm², 49 lines that had no or only a weak phenotype at this light level were repeated at 9 mW/cm² and a higher retinal concentration. 43 of these lines acquired a phenotype or a strengthened statistical significance of the previously observed phenotype under these conditions. No lines lost their phenotype at the higher intensity. (B) 10 transient locomotion lines, overlaid in the same behavior space in different colors, were repeated at the lower and higher light intensities and retinal concentrations. The boundaries of the significant regions in the behavior space shift slightly between treatments, but overall the phenotypes remain largely unchanged.